

Secondary electron emission of chemical-vapor-deposited diamond by impact of slow H^+ , D^+ , H_2^+ , C^+ , O^+ , and O_2^+ ions

M. Wieser^{a)} and P. Wurz

Physikalisches Institut, University of Bern, Sidlerstrasse 5, CH-3012 Bern, Switzerland

R. J. Nemanich

Department of Physics, North Carolina State University, 408A Cox, Box 8202, Raleigh, North Carolina 27695

S. A. Fuselier

Lockheed Research Laboratories, 3251 Hannover Street, Palo Alto, California 94304

(Received 24 February 2005; accepted 14 June 2005; published online 5 August 2005)

We report on the measurements of the secondary electron yield of chemical-vapor-deposited diamond upon the reflection of primary H^+ , D^+ , H_2^+ , C^+ , O^+ , and O_2^+ ions in an energy range of 50–1000 eV per atom at a 60° angle of incidence to the surface normal. Depending on the species and energy, a secondary electron yield between 0.1 and 2 was observed and remained unchanged over weeks without further periodic reconditioning of the surface and in spite of the moderate vacuum environment of 10^{-7} mbar. Semiempirical fit functions were found with a dependence on the inverse velocity and the square root of the atomic number of the projectiles. © 2005 American Institute of Physics. [DOI: 10.1063/1.1996855]

I. INTRODUCTION

The study of neutral gas in the magnetosphere and in the heliosphere has gained a lot of attention in recent years,^{1–3} as it allows to study remotely large plasma populations and their interactions. To investigate the spatial distributions of the neutral particle flux, a sensitive imaging neutral particle sensor is needed.^{4–7} A well-established method of detection includes imaging time-of-flight mass spectrometers as used in the neutral particle detector (NPD) in the ASPERA-3 instrument⁷ on the Mars Express spacecraft. In this type of spectrometer, start and stop pulses for time-of-flight measurement are generated by scattering the incident low-energy neutral atoms at suitable surfaces and collecting the generated secondary electrons. Combined with an energy measurement, this can be used to determine the mass of the particle. However, only limited data about secondary electron yields of materials suitable for start and stop surfaces are available in the energy range of a few eV up to 1 keV per atom. Chemical-vapor-deposited (CVD) diamond was identified as a promising secondary electron emitting surface as besides the secondary electron yield, it may also be polished to a roughness of a few nanometer rms, providing good angular scattering properties for impinging particles, and it is chemically stable. We present measurements of the secondary electron yield at a fixed angle of incidence for an energy range of 50–1000 eV per atom and for different species.

II. EXPERIMENT

A. Setup

The imager for low energetic neutral atoms (ILENA) experiment at the University of Bern (Fig. 1) consists of a

Nier-type ion source, a sector magnet for mass selection, a beam guiding and modulation system, a sample stage with housing, and a retarding potential analyzer (RPA) followed by an imaging microchannel-plate (MCP) assembly. All these units are contained in a single vacuum chamber pumped by a turbomolecular and an ion getter pump. After baking out the vacuum chamber a residual gas pressure of 4×10^{-8} mbar is achieved. During operation the pressure may rise into the low 10^{-7} -mbar range as a result of the test gas leaking into the ion source chamber. The ion source is floatable to a positive high voltage to adjust the ion energy in the range from 30 eV to 3 keV per charge. The mass per charge selection is done in a sector magnet providing a mass resolution $m/\Delta m \approx 45$. The ion-beam diameter when entering the sample housing is about 1 mm. The impact angle of the ion beam on the surface under investigation can be varied between 90° and 0° with respect to the surface normal. The RPA/MCP unit is used to investigate the charge state fractions as well as the angular distributions of the scattered particles.

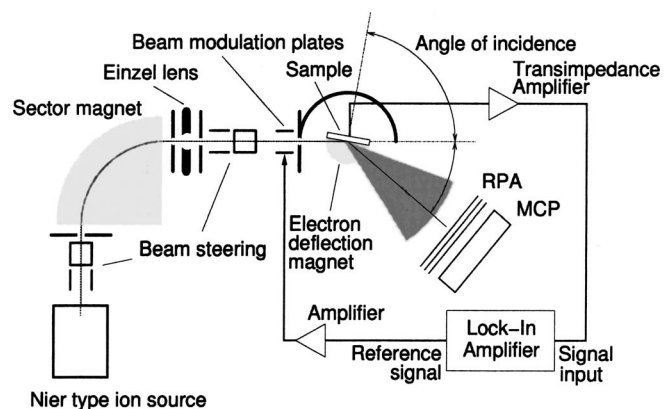


FIG. 1. ILENA experiment.

^{a)}FAX: +41 31 631 44 05; electronic mail: wieser@phim.unibe.ch

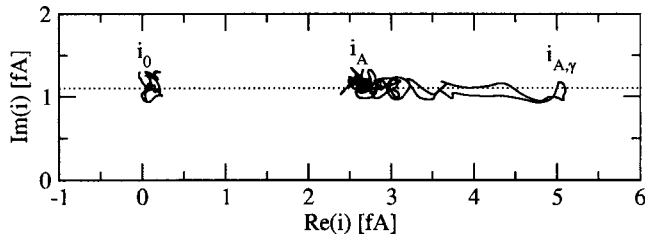


FIG. 2. Data set on the right: Value of current vector \mathbf{i} measured by the lock-in amplifier while sweeping the magnetic field at the sample from pointing upwards to downwards. A 486-eV H^+ beam impinging at 60° to the surface normal was used. The reference signal used for beam modulation points in the positive $\text{Re}(\mathbf{i})$ direction. The capacitively coupled imaginary component $\text{Im}(\mathbf{i})$ remains independent of the magnetic field whereas the real component $\text{Re}(\mathbf{i})$ varies between i_A , where the magnetic field is strong enough to hinder electrons from escaping from the surface, and $i_{A,\gamma}$ where the field is zero. Data set on the left: Without the beam, $\text{Re}(\mathbf{i})$ is very close to zero and only the capacitively coupled component i_0 of the signal remains.

The electrical current imposed onto the sample by the ion beam is measured using a Perkin Elmer 7265 lock-in amplifier. The ion-beam intensity is modulated at a frequency of 3.14 Hz by applying the reference signal of the lock-in amplifier to an additional pair of deflection plates followed by a pinhole creating a sinusoidal intensity modulation. The current \mathbf{i} onto the sample is picked up by a Femto LCA-30-1T transimpedance preamplifier and fed back into the lock-in amplifier. Only the current component in phase with the beam modulation signal, $\text{Re}(\mathbf{i})$, is considered. Capacitive coupling between the modulation signal and the sample current measurement wires produces an additional contribution $\text{Im}(\mathbf{i})$ to the measured current, which is separated in the lock-in amplifier by the 90° phase shift relative to the reference signal. Figure 2 shows data of the background signal and an actual measurement recorded with this system. Careful electrical shielding and grounding and mechanical vibration damping of the experiment allows to lock onto the signal for amplitudes down to 0.3 fA.

An adjustable magnetic field ranging from -3 to 3 mT parallel to the sample surface and normal to the primary beam allows to inhibit the escape of secondary electrons from the surface. Electrons with energies of a few eV return with a radius of gyration of a few millimeters to the surface. This is used to separate the contribution of the secondary electrons to the sample current. Compared to applying an electrostatic bias potential to the sample to retain the secondary electrons, magnetic deflection allows to selectively suppress only electrons and to keep the influence on ions negligible.

B. Surface

The surface investigated was supplied by the North Carolina State University. A 200-nm-thick boron-doped CVD diamond layer was deposited on a Si wafer and polished to a smoothness $< 10 \text{ \AA}_{\text{rms}}$. The surface was hydrogen terminated by exposing it to a hydrogen atmosphere at a temperature of a few hundred degrees Celsius.

C. Secondary electron yield

For singly positive charged projectiles, the velocity-dependent secondary electron yield $\gamma(\nu)$ is given by

$$\gamma(\nu) = \left[\frac{\text{Re}(\mathbf{i}_{A,\gamma})}{\text{Re}(\mathbf{i}_A)} - 1 \right] (1+k) \begin{cases} \text{H}^+, \text{D}^+, \text{C}^+: & k=0 \\ \text{O}^+: & k = \eta_a^-(\nu), \end{cases} \quad (1)$$

with \mathbf{i}_A the current onto the sample with a parallel magnetic field (i.e., the primary ion current), $\mathbf{i}_{A,\gamma}$ the current without magnetic field, and k a small correction for the fraction of particles ionized upon reflection of the surface. For hydrogen and carbon, positive and negative charge state fractions are both less than 0.03 per incident atom⁸ and cancel approximately ($k \approx 0$). For primary oxygen the positive charge state fraction is below 0.01 per atom and the negative charge state fraction $\eta_a^-(\nu)$ dominates; however, its value is below 0.2 per atom.⁸ For molecular projectiles H_2^+ and O_2^+ , it was assumed according to the data reported in Refs. 9 and 10 that a molecule produces the same amount of secondary electrons as its equally fast constituents:

$$\gamma_M(\nu) \approx \sum \gamma_A(\nu) = 2\gamma_A(\nu). \quad (2)$$

Charge state fractions per atom obtained from hydrogen and oxygen molecules are similar to the charge state fractions obtained from equally fast atoms.⁸ For H_2^+ and O_2^+ molecules, the secondary electron yield per atom is thus obtained by

$$\gamma(\nu) = \frac{1}{2} \left[\frac{\text{Re}(\mathbf{i}_{M,\gamma})}{\text{Re}(\mathbf{i}_M)} - 1 \right] (1+2k), \quad (3)$$

with \mathbf{i}_M the current onto the sample with a parallel magnetic field, $\mathbf{i}_{M,\gamma}$ the current without magnetic field, and k the correction for the ionized fraction of the reflected particles as in Eq. (1).

III. RESULTS AND DISCUSSION

Both Eqs. (1) and (3) allow the determination of the secondary electron yield using two current measurements, aside from the need of knowledge on the negative ion yield in the case of oxygen. The two current values are obtained by scanning the magnetic field from negative (field pointing downwards) to positive values (field pointing upwards) as shown in Fig. 3.

The secondary electron yield per atom, γ , for all investigated species is shown in Fig. 4. For H^+ and H_2^+ , the assumption from Eq. (2) is well justified *a posteriori*. For oxygen, however, Eq. (2) does not reproduce the data well. The secondary electron yield per atom obtained from O_2^+ was larger by a factor of 1.7 compared to O^+ . This is in contrast to the data obtained from thin carbon foils¹¹ where a factor less than 1 is observed. Within measurement errors, no isotopic dependency of γ could be found between H^+ and D^+ in the investigated velocity range. The values reported for C^+ fit well in the general trend of a higher γ for a larger atomic number Z of the projectile. A semiempirical fit function of the form

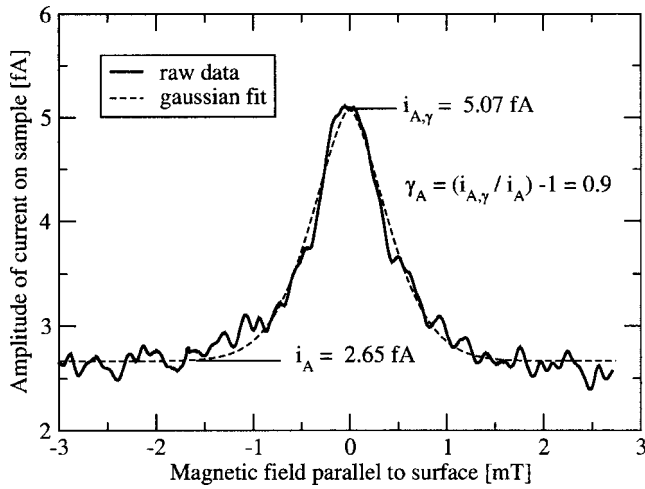


FIG. 3. Sample current depending on magnetic-field strength. A 486-eV H^+ beam impinging at 60° to the surface normal was used.

$$\gamma = \gamma_0 e^{-\nu_0 k / \nu \sqrt{Z}} \quad (4)$$

was applied to the data, with ν the particle velocity, $\nu_0 = \alpha c = 2.18 \times 10^7$ m/s, k a projectile species independent fitted constant equal to 0.215, and γ_0 a free parameter depending on projectile species representing the secondary electron yield per atom obtained from Eq. (4) for the asymptotic case $\nu \rightarrow \infty$. Table I depicts the values found for γ_0 depending on the projectile type. These fits are plotted in Fig. 4 as solid lines.

An approximation for higher velocities is obtained by expanding Eq. (4) to a series around $\nu = \nu_0 k$,

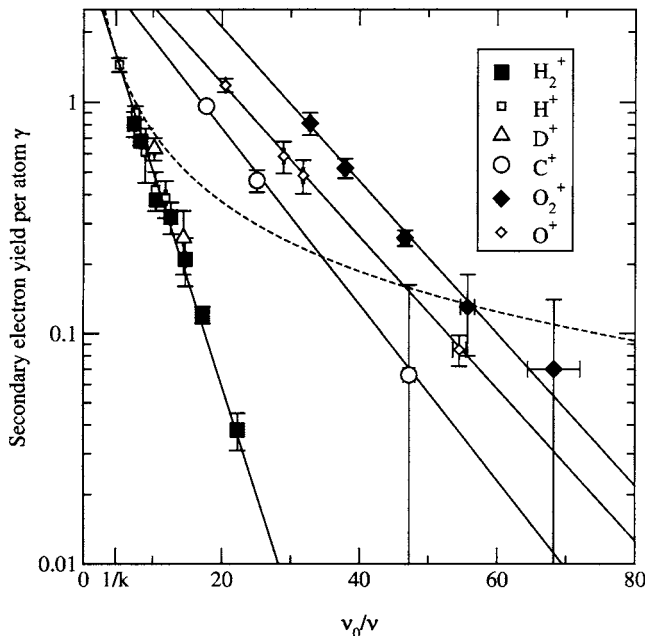


FIG. 4. Secondary electron yield for various primary particles impinging at 60° to the surface normal. Fits using Eq. (4) with parameters from Table I are shown as solid lines. The dashed line shows the linear approximation obtained for $\nu_0 / \nu = 1/k$ used in the series expansion in Eq. (5).

TABLE I. Fit parameters for Eq. (4) used in Fig. 4. γ_0 is given in units of secondary electrons per atom.

Projectile	γ_0
H^+, D^+, H_2^+	4.35
C^+	4.46
O^+	5.51
O_2^+	9.56

$$\gamma \approx \gamma_0 \left(1 - \frac{1}{\sqrt{Z}} \right) e^{-1/\sqrt{Z}} + \frac{\nu}{\nu_0 k} \frac{\gamma_0}{\sqrt{Z}} e^{-1/\sqrt{Z}} + \dots = a + \frac{\nu}{\nu_0} b + \dots, \quad (5)$$

which shows the linear dependence of γ with the projectile velocity ν at higher particle velocities. For hydrogen, the constant term a in Eq. (5) vanishes, reducing the equation to $\gamma \sim \nu$, which is a well-known relation for a kinetic secondary electron emission. The secondary electron emission γ is generally thought to be proportional to the electronic stopping power S_e ,¹² and S_e being proportional to ν in the Lindhard-Scharff velocity regime $\nu \leq Z^{2/3} \nu_0$.¹³ This condition is satisfied for all investigated species for $\nu = \nu_0 k$, because k is smaller than 1. However, at lower velocities γ is overestimated when using $\gamma \sim \nu$ (see dashed line in Fig. 4) and better fits to the data are obtained using Eq. (4). A dependence of $\gamma \sim e^{-A/\nu_\perp}$ with A being a constant and ν_\perp the velocity of the projectile perpendicular to the surface was also reported in Ref. 14 where a surface electron-hole pair excitation mechanism was identified for the emission of secondary electrons from slow Li^+ ions impinging on aluminum; however, no projectile-type dependence was reported there. For data reported in Refs. 15 and 16 for C^+ , N^+ , and O^+ impinging on a polycrystalline gold surface, surface-assisted kinetic electron emission is identified as a dominant mechanism for electron emission. These data are also well fitted with the fit function shown in Eq. (4). Similar to the findings reported in Ref. 17, our data do not show a threshold velocity for secondary electron emission.

IV. CONCLUSION

The measurement of the secondary electron yield by suppressing electrons by a magnetic field is advantageous compared to biasing the sample electrostatically at low ion energies. The energy and trajectory of the primary ions is not changed noticeably by the magnetic field. The secondary electron yields found for CVD diamond for the species investigated were well fitted by an empirical fit function [Eq. (4)] showing a dependence from the inverse velocity and the square root of the atomic number of the projectile.

ACKNOWLEDGMENT

The financial support by the Swiss National Science Foundation is acknowledged.

¹P. Wurz, *The Outer Heliosphere: Beyond the Planets* (Copernicus Gesellschaft e.V., Katlenburg-Lindau, Germany, 2000), Chap. 11.

²H.-J. Fahr, *Adv. Space Res.* **34**, 3 (2004).

³M. Witte, M. Banaszkiewicz, H. Rosenbauer, and D. McMullin, *Adv.*

Space Res. **34**, 61 (2004).

⁴D. J. McComas *et al.*, in *Physics of the Outer Heliosphere: Third International IGPP Conference*, edited by V. Florinski, N. Pogorelov, and G. Zank, AIP Conf. Proc. No. 719 (AIP, Melville, NY, 2004), pp. 162–181.

⁵M. Witte, H. Rosenbauer, E. Keppler, H. Fahr, P. Hemmerich, H. Lauche, A. Loidl, and R. Zwick, *Astron. Astrophys.* **92**, 333 (1992).

⁶T. Moore *et al.*, *Space Sci. Rev.* **91**, 155 (2000).

⁷S. Barabash *et al.*, Eur. Space Agency, [Spec. Publ.] ESA SP **1240**, 121 (2004).

⁸J. Scheer *et al.*, *Nucl. Instrum. Methods Phys. Res. B* **230**, 330 (2005).

⁹B. Svensson, G. Holmén, and J. Linnros, *Nucl. Instrum. Methods Phys. Res.* **194**, 429 (1982).

¹⁰E. S. Chambers, *Phys. Rev.* **133**, A1202 (1964).

¹¹S. M. Ritzau and R. A. Baragiola, *Phys. Rev. B* **58**, 2529 (1998).

¹²R. Baragiola, *Nucl. Instrum. Methods Phys. Res. B* **78**, 233 (1993).

¹³G. Betz and K. Wien, *Int. J. Mass Spectrom. Ion Processes* **140**, 1 (1994).

¹⁴J. Yarmoff, T. Liu, S. Qiu, and Z. Sroubek, *Phys. Rev. Lett.* **80**, 2469 (1998).

¹⁵H. Eder, F. Aumayer, and H. Winter, *Nucl. Instrum. Methods Phys. Res. B* **154**, 185 (1999).

¹⁶J. Lörincik, Z. Sroubek, H. Eder, F. Aumayr, and H. Winter, *Phys. Rev. B* **62**, 16116 (2000).

¹⁷J. Lörincik, Z. Sroubek, S. Cernusca, A. Diem, H. Winter, and F. Aumayr, *Surf. Sci.* **504**, 59 (2002).